


# Combined Prussian Blue Nanozyme Carriers Improve Photodynamic Therapy and Effective Interruption of Tumor Metastasis

Wenhao Shen<sup>1,\*</sup>, Gaohua Han<sup>1,\*</sup>, Lei Yu<sup>1</sup>, Song Yang<sup>1</sup>, Xiangyi Li<sup>2</sup>, Wei Zhang<sup>3</sup>, Pei Pei<sup>4</sup> 

<sup>1</sup>Department of Oncology, Hospital Affiliated 5 to Nantong University (Taizhou People's Hospital), Taizhou, Jiangsu, People's Republic of China;

<sup>2</sup>Department of Endocrinology, Hospital Affiliated 5 to Nantong University (Taizhou People's Hospital), Taizhou, Jiangsu, People's Republic of China;

<sup>3</sup>Department of Infectious Disease, Hospital Affiliated 5 to Nantong University (Taizhou People's Hospital), Taizhou, Jiangsu, People's Republic of China;

<sup>4</sup>School of Basic Medical Sciences, Anhui Medical University, Hefei, 230032, People's Republic of China

\*These authors contributed equally to this work

Correspondence: Wei Zhang; Pei Pei, Email [zw562652291@126.com](mailto:zw562652291@126.com); [ppei1204@outlook.com](mailto:ppei1204@outlook.com)

**Introduction:** Photodynamic therapy (PDT) as a new technique for theranostics is to kill tumor cells by activating photosensitizer and interacting with oxygen (O<sub>2</sub>) to produce reactive oxygen species (ROS). However, the hypoxic tumor microenvironment (TME) may constrain the efficacy of PDT. Moreover, the lack of O<sub>2</sub> in TME also up-regulates the expression of HIF-1 $\alpha$  and promotes tumor metastasis, which is also a leading cause of death for terminal cancer patients.

**Methods:** Prussian blue (PBs) was firstly synthesized by hydrothermal method, which was then etched by hydrochloric acid to obtain hollow Prussian blue nanoparticles (HPBs). Afterwards, Au-Pt nanozymes were in situ growing on the HPBs by reduction method to prepare Au-Pt@HPBs (APHPBs). Owing to the hollow structure of APHPBs, photosensitizer Ce6 can be easily and efficiently loaded into it to obtain Ce6-Au-Pt@HPBs (Ce6-APHPBs). After ce6-APHPBs regulation, photoacoustic imaging and hypoxic fluorescence imaging were then used to evaluate changes in hypoxic TME in vivo. Finally, under the assistant of Ce6-APHPBs, we evaluated the inhibitory effect of enhanced PDT on primary and metastatic tumors.

**Results:** We first designed and synthesized Ce6 loaded hollow prussian blue nanoparticles with Au-Pt nanozymes grown in situ on it. Both in vitro and in vivo experiments show that the prepared Ce6-APHPBs have good biosafety and could effectively degrade the overexpressed H<sub>2</sub>O<sub>2</sub> in TME to generate O<sub>2</sub>, further relieve the hypoxic TME and thus enhance the effect of PDT. At the same time, the increasing O<sub>2</sub> content could also reduce the expression of HIF-1 $\alpha$  at the tumor site, which could reduce lung metastasis.

**Conclusion:** Ce6-APHPBs designed by us could not only efficiently enhance PDT but also regulate TME to reduce tumor metastasis and prolong survival of mice, which provide a novel idea and strategy for clinical PDT and metastatic tumor.

**Keywords:** Au-Pt nanozymes, prussian blue, enhanced PDT, TME, HIF-1 $\alpha$ , tumor metastasis

## Introduction

Tumor recurrence and metastasis are primary reasons for high cancer mortality.<sup>1-3</sup> Tumor metastasis and growth are closely related to the hypoxic tumor microenvironment (TME), which can activate hypoxia inducible factor-1 (HIF-1 $\alpha$ ), along with the upregulation of relevant genes, such as tumor proliferation, survival, metabolism, angiogenesis and drug-resistant genes, affecting the therapeutic effect of cancer.<sup>4-9</sup> Hence, effective tumor therapy requires not only effective inhibition of tumor growth in situ but also effective improvement of the TME to restrain tumor recurrence and metastasis.<sup>10-12</sup>

Being different from the traditional therapies, such as surgery, chemotherapy and radiotherapy, photodynamic therapy (PDT) uses a photosensitizer to transfer laser energy to oxygen molecules to generate reactive oxygen species (ROS) to kill cancer cells.<sup>13-17</sup> PDT offers apparent advantages of being noninvasive, exhibiting non drug resistance with few side effects and becomes an important treatment of cancer.<sup>18-21</sup> However, the low delivery efficiency of photosensitizers in vivo and the high dependence on oxygen limit its therapeutic effect on hypoxic solid tumors.<sup>22-25</sup> Therefore, to face challenges in the

clinical application of PDT, we need to find an effective method for the delivery of photosensitizer and oxygen to improve the efficacy and inhibit tumor recurrence and metastasis.<sup>26,27</sup> At present, the ways to remit hypoxic TME include hyperbaric oxygen chambers, delivery of oxygen-containing perfluorides and decomposition of tumor endogenous hydrogen peroxide ( $H_2O_2$ ) to produce oxygen by nanoenzyme catalase activity.<sup>28–31</sup> Nanoenzymes have been widely used in combination therapy for improving the TME due to their low price and high catalytic activity.<sup>32</sup>

Prussian blue has been approved by the US Food and Drug Administration (FDA) as a clinical antidote for thallium and other radioactive element poisoning.<sup>33,34</sup> It is excellent biological safety, high stability and easy of preparation, and its unique hexacyanohydrate skeleton structure gives it the ability to load hydrophobic drugs.<sup>35,36</sup> Studies have shown that hollow Prussian blue nanoparticles can effectively load chemotherapy drugs and be used for tumor-targeted thermochemotherapy.<sup>37–42</sup> In addition, Prussian blue nanoparticles have the potential to be highly effective drug carriers due to their stable structure, good stability and long blood circulation time.<sup>43,44</sup>

In our work, Prussian blue were synthesized by hydrothermal method firstly and then etched by HCl to obtain hollow Prussian blue (HPBs). Subsequently, we grew Au-Pt in situ on the hollow prussian blue by reduction method the first time. Hollow prussian prussian blue nanozyme particles (AuPt@HPBs) with high catalase activity were obtained. Finally, the photosensitizer chlorin e6 (Ce6) was successfully loaded into hollow prussian blue nanozyme particles to obtain Ce6-Au-Pt@HPB nanoparticles (Ce6-APHPBs), which can not only significantly improve the hypoxic micro-environment of tumors but also improve the blood oxygen saturation of tumors and effectively reduce the expression of HIF-1 $\alpha$  in tumor cells. After 660 nm irradiation, Ce6-APHPBs can produce more singlet oxygen, remove the limitation of hypoxic oxygen on photodynamic therapy, and effectively inhibit tumor growth. More importantly, this treatment strategy can not only significantly inhibit the growth of tumors in situ but also greatly reduce tumor metastasis and prolong the life cycle of mice. In conclusion, the new type hollow Prussian blue nanozyme particles we developed provide a novel idea and strategy for killing two birds with one stone for clinical photodynamic therapy and metastatic tumor.

## Materials and Methods

$K_3[Fe(CN)_6] \cdot 3H_2O$ , PVP and hydrochloric acid were purchased from Sigma–Aldrich. Chlorin e6 (Ce6) was obtained from Cayman. Antibodies for tissue slices were obtained from Abclonal. The HypoxyprobeTM-1 Plus Kit was purchased from Hypoxyprobe, Inc. Morphology was characterized by a Tecnai G2 spirit BioTwin transmission electron microscope. The hydrodynamic diameters and zeta potentials were characterized by a Zetasizer Nano ZS90. Photoacoustic images were collected from MSOT inSight/inVision 256. The oxygen content in the  $O_2$  generation curve was detected by portable dissolved oxygen meters (JPBJ-608, Shanghai REX Instrument Factory).

## Synthesis of Prussian Blue Nanoparticles

Briefly, 131.72 mg  $K_3[Fe(CN)_6] \cdot 3H_2O$  and 3 g PVP were added to 40 mL hydrochloric acid (HCl) aqueous solution (1 M) and stirred magnetically for 30 min. Next, the mixture was put into an oven heated to 80 °C for 24 h, and Prussian blue nanoparticles (PBs) were obtained through vacuum drying for 24 h after collection by centrifugation (17,000 rpm, 15 min, Beckman, Optima L-100XP) and washing with ethanol 3 times.

## Synthesis of Hollow Prussian Blue Nanoparticles

PBs (12 mg) and PVP (120 mg) were added to HCl solution (12 mL, 1 M) and stirred for 4 h followed by heating in a muffle furnace (140°C, 2 h). After cooling to room temperature, the HPBs were gathered through centrifugation (13,000 rpm, 20 min) and cleaned with ethanol 3 times after vacuum drying overnight.

## In situ Growth of Au-Pt Nano-Enzyme on Hollow Prussian Blue

One milliliter of HPBs solution was first dispersed in 15 mL deionized (DI) water, and then the above solution was mixed with 3.25  $\mu$ L  $HAuCl_4 \cdot 4H_2O$  (1 M) and  $H_2PtCl_6 \cdot 6H_2O$  (1 M) with generous stirring. After that, 1 mL  $NaBH_4$  (1 mg/mL) ice-cold solution was slowly put into the commixture. Finally, APHPBs were obtained by washing with DI water several times and dispersed in DI water for further use.

## Preparation of Chlorin e6 Loaded Au-Pt Nano-Enzyme Hollow Prussian Blue

HPBs and APHPBs (1 mL, 10 mg/mL) were mixed with 1 mg Ce6 and magnetically stirred overnight. Ce6-HPBs and Ce6-APHPBs were obtained after washing with DI water 3 times. The load rate of Ce6 in Ce6-HPBs and Ce6-APHPBs was  $4.07 \pm 0.13\%$  (wt./wt.) and  $4.01 \pm 0.62\%$  (wt./wt.), respectively, which was detected by ultraviolet (UV) spectrophotometry at an absorption of 405 nm.

## In vitro Drugs Release of Chlorin e6 Loaded Au-Pt Nano-Enzyme Hollow Prussian Blue

The release of Ce6 in nanoparticles was conducted under different conditions (pH=6.5 and pH=7.4). Ce6-HPBs (1 mL) and Ce6-APHPBs (Ce6: 100  $\mu\text{g/mL}$ ) were placed in dialysis bags, which were then placed in reaction bottles containing 15 mL PBS (pH 7.4 and pH 6.5), respectively. At each time point, 1 mL of liquid was taken to measure the UV absorption of Ce6 (405 nm) in each group at different time points, and then the same amount of PBS was added to the reaction system.

## Detection of Oxygen Production

Portable dissolved oxygen meters were used to measure the dissolved oxygen concentration. Generally, PBS, HPBs (100  $\mu\text{g/mL}$ ) and Ce6-APHPBs (100  $\mu\text{g/mL}$ ) were mixed with  $\text{H}_2\text{O}_2$  solution to a final  $\text{H}_2\text{O}_2$  concentration of 5 mM. After that,  $\text{O}_2$  generation at different time points was detected by portable dissolved oxygen meters.

## Detection of Singlet Oxygen Generation

9.10-Anthracenediyl-bis(methylene)dimalonic acid (ABDA) was used to evaluate the ability of Ce6-HPBs and Ce6-APHPBs to generate  $^1\text{O}_2$  since 9.10-anthracyl-bis(methylene) dimalonic acid can react quickly with anthracene to capture ROS effectively. Briefly, 100  $\mu\text{L}$  of 0.1 mg/mL ABDA (pH=7.4) was put into different groups (PBS, Ce6-HPBs, Ce6-APHPBs, Ce6-HPBs plus 660 nm, Ce6-APHPBs plus 660 nm, Ce6-HPBs plus  $\text{H}_2\text{O}_2$  plus 660 nm, Ce6-APHPBs plus  $\text{H}_2\text{O}_2$  plus 660 nm) (the illumination group was illuminated with a 660 nm wavelength (300  $\text{mW/cm}^2$ , 1 min at a time)). The above groups were then mixed with ABDA phosphate buffer solution (pH 7.4, 2 mL). We can detect the absorption peak of 9.10-anthracyl-bis(methylene)dimalonic acid (379 nm) to reflect the ROS production effect and then translate it into ROS production capacity.

## Cell Line and Animals

Cells of the human vascular endothelial cell line (HUVECs) and murine breast cancer cell line (4T1 cells) were supported by the central laboratory of Taizhou People's Hospital (purchased from the Cell Bank, Shanghai Institutes for Biological Sciences, Chinese Academy of Sciences, Shanghai). Cell culture medium were purchased from Shanghai QiDa Biotechnology Co., LTD. Female BALB-c mice (6–8 weeks) were obtained according to protocols approved by the Nantong University Laboratory Animal Center. All animal protocols were in accordance with the National Institute's Health Guide for the Care and Use of Laboratory Animals.

## Cell Experiments

Cell cytotoxicity was detected by the Cell Counting Kit-8 (CCK-8) assay (purchased from Sigma, Shanghai). DCFH-DA for detecting reactive oxygen species (ROS) generated by Ce6-HPBs and Ce6-APHPBs after irradiation (irradiation time: 8 min, 300  $\text{mW/cm}^2$ ) was purchased from Beyotime. Fluorescence microscopy images of live/dead stained 4T1 cells after treatment with different formulations (irradiation time: 8 min, 300  $\text{mW/cm}^2$ ). The fluorescence images were analysed using IVIS. Live/dead cell trials were conducted using a CA/PI staining kit (Beyotime).

## Ex vivo Analysis of Immunofluorescence Slices

4T1 tumor-bearing mice were injected through the tail vein with PBS and Ce6-APHPBs (200  $\mu$ L, 2 mg/mL) at days 1 and 3. Then, mice were sacrificed to obtain tumor slices that were stained with Ki67 (A11390, Abclonal), Myc-Tag (AE070, Abclonal), anti-HIF-1 $\alpha$  (ab179483, Abcam) and DAPI (ab228549, Abcam) antibodies at day 4. The c-Myc and HIF-1 $\alpha$  levels of regulatory T cells in tumor cells were also analysed by flow cytometry. In detail, cells were first stained with the following surface antibodies: anti-CD3-FITC (eBioscience, Clone: 17A2, 11-0032-82) and anti-CD4-PerCP. After fixation and permeabilization, cells were stained with anti-FoxP3-PE (eBioscience, Clone: NRRF-30, 72-5775-40), anti-HIF-1 $\alpha$ -APC (Thermo Fisher, Clone: Mgc3, 17-7528-82) and anti-Myc-Alexa Fluor 647 (ab223895, Abcam) and then analysed by flow cytometry.

## In vivo Antitumor of Chlorin e6 Loaded Au-Pt Nano-Enzyme Hollow Prussian Blue

Healthy BALB/c mice with 4T1 tumors were randomly divided into four groups: (1) PBS; (2) Ce6 plus 660 nm; (3) Ce6-HPBs plus 660 nm; and (4) Ce6-APHPBs plus 660 nm ([Ce6: 8 mg/kg], [HPBs: 20 mg/kg] and [APHPBs: 20 mg/kg]). When the tumor volume reached 50–100 mm<sup>3</sup> postinjection in the different groups. The tumor size and mouse weight were recorded every other day for 14 days. The survival rates of each group were recorded for up to 30 days. The mice were deemed to be dead until the tumor volume reached 1000 mm<sup>3</sup> (volume = [length\*width<sup>2</sup>]/2). Mice in each group were sacrificed on day 14 to gather the tumors and mean organs for hematoxylin and eosin (H&E) staining and on day 7 to obtain TUNEL-stained tumor slices after specific treatment. Mice in each group were sacrificed to obtain lung slices for H&E staining after various treatments for 20 days.

## Results and Discussion

The synthetic procedures and mechanism of enhanced PDT for inhibiting tumor growth and reducing metastasis to the lung are shown in [Figure 1A](#). Firstly, PBs were synthesised using the method in the previous literature. Then, hollow HPBs are formed by acid etching of PBs. Finally, Au-Pt nanoparticles were grown on HPBs in situ forming APHPBs which were then mixed with FDA-approved Ce6 to generate Ce6-APHPBs. Ce6-APHPBs were injected into mice through the tail vein and enriched in tumor cells by the enhanced permeability and retention (EPR) effect. The overexpressed hydrogen peroxide (H<sub>2</sub>O<sub>2</sub>) was decomposed into water (H<sub>2</sub>O) and oxygen (O<sub>2</sub>) with Au-Pt for catalysis. Moreover, the PDT effect induced by Ce6 was significantly improved with 660 nm laser irradiation, downregulating the expression of HIF-1 $\alpha$  and reducing lung metastasis. The morphology of PBs, HPBs, APHPBs and Ce6-APHPBs were investigated by transmission electron microscope (TEM). As shown in [Figure 1B](#), the synthesized PBs was in regular cube structure. The acid etched some pore volume in HPBs for loading photosensitizer Ce6. Besides, the Au-Pt nanozyme were also distributed on the surface of HPBs evenly. The dynamic light scattering (DLS) showed that the particle size of HPBs was ~105 nm, and the particle size of the hydrated Au-Pt nanoenzyme was increased to ~110 nm after in situ synthesis, and the particle size of Ce6-APHPBs after loading Ce6 was ~110 nm ([Figure 1C](#)). These results were consistent with the previous electron microscope size. Then, APHPBs were mixed with Ce6 and magnetically stirred overnight. The UV-Vis results showed that Ce6-APHPBs contained the characteristic absorption peak of Ce6, indicating that Ce6 was successfully loaded into hollow prussian blue ([Figure 1D](#)). In addition, the zeta potential of HPBs was -13.36 mV, which then changed to -30.6 mV and -33.5 mV after loading nanozyme and Ce6, indicating that the Au-Pt nanozyme and Ce6 were successfully loaded on HPBs ([Figure 1E](#)). Subsequently, we investigated the drug release capacity of Ce6-APHPBs under different pH conditions (pH=7.4 and pH=5.6). Ce6-HPBs could release 47.2% of Ce6 and Ce6-APHPBs could release 50.3% of Ce6 under neutral conditions (pH=7.4). Ce6-HPBs could release 81.8% of Ce6 and Ce6-APHPBs could release 84.4% of drugs under acidic conditions (pH=6.5). These results indicated that Ce6-APHPBs could release more drugs at the tumor site with acidic condition ([Figure 1F](#)).

Based on the above, we successfully prepared Ce6-APHPBs and proved that it has efficient drug loading capacity and drug release ability. Next, we verified whether Ce6-APHPBs could effectively decompose H<sub>2</sub>O<sub>2</sub> and produce cellular reactive oxygen species (ROS). The photosensitizer Ce6 was photoexcited by 660 nm light and converted the oxygen



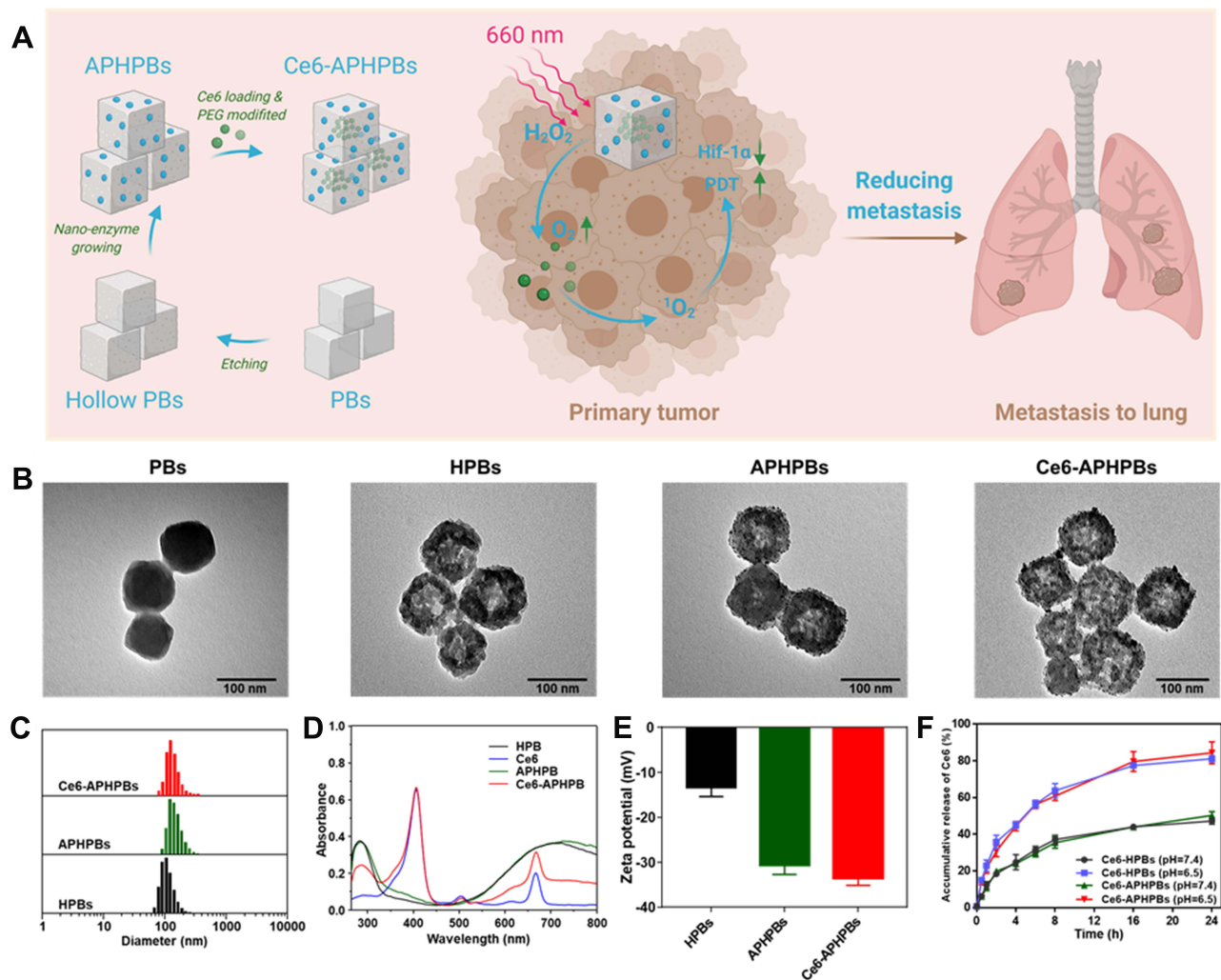
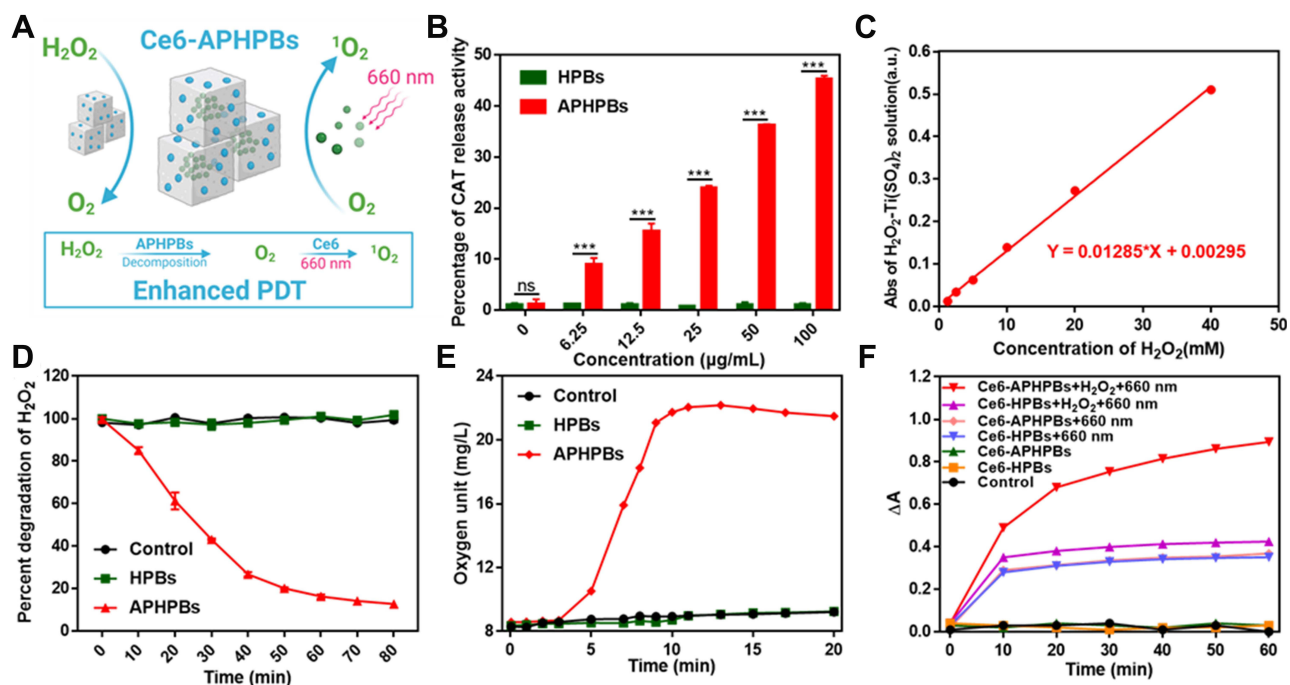


**Figure 1** (A) Schematic illustration of the synthesis procedure of Ce6-APHPBs and the mechanism of enhanced PDT for inhibiting tumor growth and reducing metastasis to the lung. Created with BioRender.com. (B) Transmission electron microscopy (TEM) images of Prussian blue (PBs), hollow Prussian blue (HPBs), hollow Prussian blue with in situ growth of Au-Pt (AHPBs) and Ce6-loaded hollow Prussian blue with in situ growth of Au-Pt (Ce6-APHPBs). (C) Dynamic light scattering (DLS) of HPBs, AHPBs and Ce6-APHPBs. (D) Absorbance spectra of HPB, free Ce6, AHPBs and Ce6-APHPBs. (E) Zeta potential of HPBs, AHPBs and Ce6-APHPBs. Error bars represent mean  $\pm$  s. d. (n = 3) (F) Accumulative release of Ce6 in Ce6-HPBs and Ce6-APHPBs under different conditions (pH=6.5 and pH=7.4) over 24 h. Error bars represent mean  $\pm$  s. d. (n = 3).

generated by the degradation of H<sub>2</sub>O<sub>2</sub> into singlet oxygen (<sup>1</sup>O<sub>2</sub>), then killed tumor cells (Figure 2A). Based on this mechanism, we firstly evaluated the catalase activity of AHPBs at different concentration by Micro Catalase (CAT) Assay Kit. With increasing concentration of HPBs and AHPBs, the enzyme activity of HPBs decreased, while the enzyme activity of AHPBs increased step by step, which suggests that AHPBs have better catalytic activity (Figure 2B). After that, we further used Ti(SO<sub>4</sub>)<sub>2</sub> solution to detect the degradation of H<sub>2</sub>O<sub>2</sub>, since Ti(SO<sub>4</sub>)<sub>2</sub> could react with H<sub>2</sub>O<sub>2</sub> to produce H<sub>2</sub>O<sub>2</sub>-Ti(SO<sub>4</sub>)<sub>2</sub>, which has a UV characteristic absorption peak (405 nm). There was also an obvious linear regression of the content of H<sub>2</sub>O<sub>2</sub>-Ti(SO<sub>4</sub>)<sub>2</sub> with different concentrations of H<sub>2</sub>O<sub>2</sub> (Figure 2C). AHPBs could degrade H<sub>2</sub>O<sub>2</sub> rapidly within 80 min, while the control group (PBS and HPBs) had almost no catalytic ability to degrade H<sub>2</sub>O<sub>2</sub> (Figure 2D). Subsequently, the ability of AHPBs to catalyze H<sub>2</sub>O<sub>2</sub> to produce oxygen was investigated. A portable dissolved oxygen meters was used to detect the oxygen content produced by AHPBs. The results showed that AHPBs could generate more O<sub>2</sub> during 24 min compared with PBS and HPBs (Figures 2E and S1).

To verify if Ce6-APHPBs could convert oxygen into <sup>1</sup>O<sub>2</sub> in vitro and enhance the therapeutic effect of PDT, we used 9.10-anthracenediyl-bis (methylene) dimalonic acid (ABDA) which could react quickly with anthracene to capture ROS



effectively to evaluate the ability of Ce6-HPBs and Ce6-APHPBs to generate <sup>1</sup>O<sub>2</sub>. The Ce6-APHPBs plus H<sub>2</sub>O<sub>2</sub> plus 660 nm group could produce more <sup>1</sup>O<sub>2</sub> than the other groups within 60 min (Figure 2F).

The above experiments prove that Ce6-APHPBs could effectively degrade H<sub>2</sub>O<sub>2</sub> and produce <sup>1</sup>O<sub>2</sub> in vitro. In addition, we tested the ability of Ce6-APHPBs to produce ROS at the cellular level firstly. We used DCFH-DA as an indicator that could combine with ROS to generate green fluorescence. As shown in Figure 3A, laser irradiation applied for 8 min after coincubation of 4T1 cells with Ce6-APHPBs produced more green fluorescence than the control group, indicating that Ce6-APHPBs plus 660 nm irradiation could produce more ROS. Subsequently, human umbilical vein endothelial cells (HUVECs) and 4T1 cells were used to verify the biosafety of different groups. When the concentration of APHPBs reached 200 µg/mL, both HUVECs and 4T1 cells maintained more than 80% of the cell viability, indicating that APHPBs is good biosafety (Figure 3B). Considering that Ce6-APHPBs could consume H<sub>2</sub>O<sub>2</sub> and produce oxygen, we tested the cytotoxicity of different materials under normal oxygen conditions and hypoxic conditions separately. After laser irradiation under normal oxygen conditions, the reactive oxygen species produced by materials could kill more than 50% of tumor cells. It is obvious that the cytotoxicity of the material in the condition of conventional oxygen is stronger than that in hypoxic conditions because more oxygen provides more singlet oxygen generating unit for PDT (Figure 3C and D). After that, we carried out the dead and live staining experiments, in order to reflect the cell killing ability of materials directly. The tumor cells were killed effectively in the Ce6-APHPBs plus 660 nm group, which was consistent with the results of the previous cytotoxicity experiment (Figure 3E).

Photoacoustic (PA) imaging was conducted to monitor the O<sub>2</sub> levels in the TME by monitoring oxyhemoglobin (HbO<sub>2</sub>) level at different time points to discuss the effects and mechanism of Ce6-APHPBs. Deoxyhaemoglobin (Hb) and HbO<sub>2</sub> were probed through PA imaging with excitation wavelengths of 750 and 850 nm respectively. As shown in Figure 4A and B, HbO<sub>2</sub> (red) signals were significantly increased after i.v. injection of Ce6-APHPBs, demonstrating that Ce6-APHPBs could improve the O<sub>2</sub> content, further alleviating the hypoxic tumor microenvironment. We then performed hypoxic fluorescence slices of the tumors, with the green fluorescence showing the hypoxic regions. Ce6-APHPBs

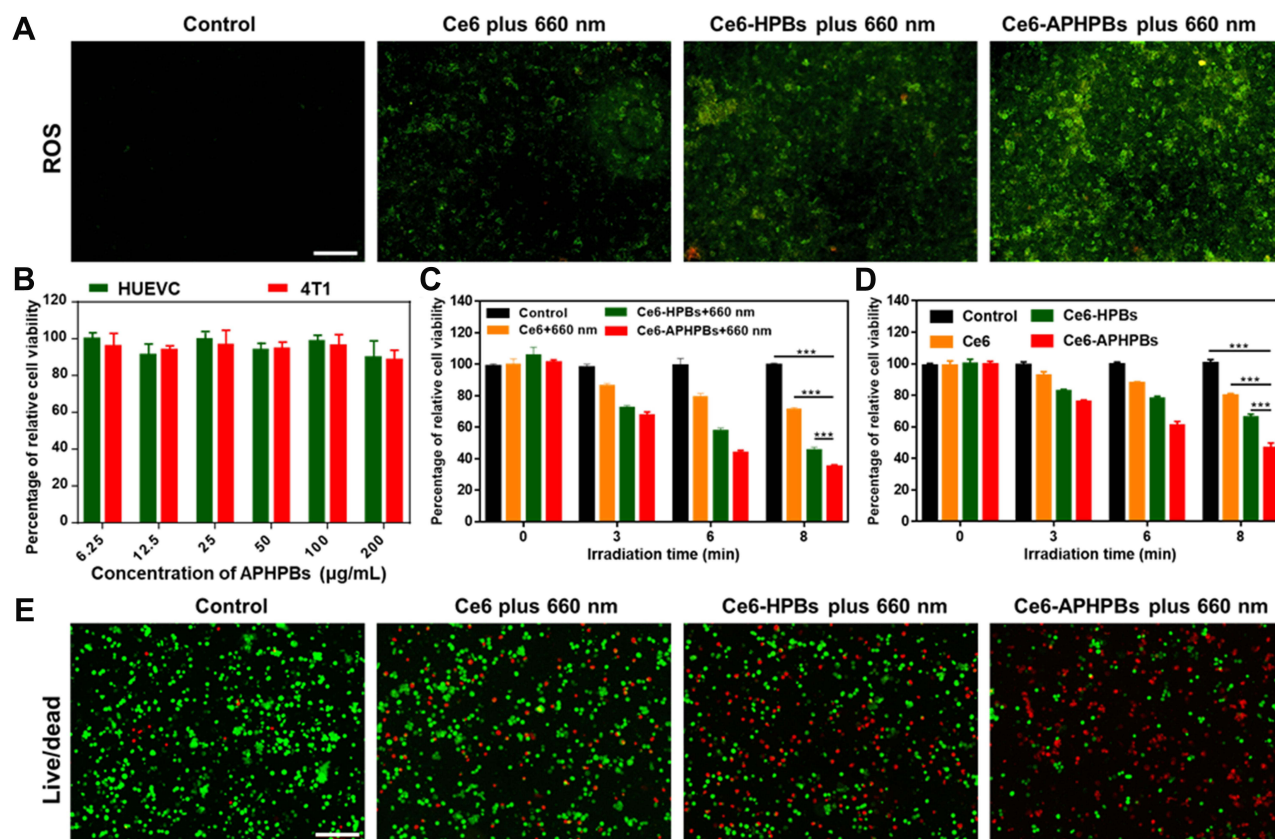


**Figure 3** (A) Fluorescence microscopy imaging of 4T1 cells stained with DCFH-DA for detecting the reactive oxygen species (ROS) after treatment with PBS, Ce6 plus 660 nm, Ce6-HPBs plus 660 nm and Ce6-APHPBs plus 660 nm (Ce6: 4 μg/mL, Ce6-HPBs: 100 μg/mL, Ce6-APHPBs: 100 μg/mL, irradiation time: 8 min). (B) Relative cell viability of HUVECs and 4T1 cells after incubation with APHPBs at different concentrations for 24 h. Error bars represent the mean ± s.d (n = 3). Relative cell viability of 4T1 cells after treatment with different methods for different irradiation times in normal oxygen (C) and hypoxia (D). Error bars represent mean ± s.d. (n = 3) (E) Fluorescence microscopy images of live/dead stained 4T1 cells after treatment with different formulations (irradiation time: 8 min, 300 mW/cm<sup>2</sup>) and for an additional 24 h incubation. P values in c and d were calculated by multiple t tests (\*\*\*) (P < 0.001).

effectively improved the hypoxic tumor microenvironment in Figure 4C, which is also consistent with previous results. Moreover, tumors were further collected and analysed by confocal microscopy for immunofluorescence staining. Notably, a significant decrease in the expression of HIF-1α was found after i.v. injection of Ce6-APHPBs, which may be due to the production of O<sub>2</sub> at tumor sites (Figure 4D).

With the results of the cellular experiments to support the work, we then focus on the experiments in vivo. Firstly, we constructed 4T1 tumor models by subcutaneously implanting 4T1 cells on the back of healthy BALB/c female mice. When the tumor volume reached approximately 100 mm<sup>3</sup>, we injected different materials into the body through the tail vein of the tumor-bearing mice every two days for a total of three injections. Twelve hours after each injection, the tumors were irradiated with a laser (660 nm) for 16 min (Figure 5A). While the Ce6-HPBs plus 660 nm group showed some tumor suppression, the Ce6-APHPBs plus 660 nm group revealed a stronger therapeutic effect (Figure 5B and C). Moreover, the survival rate of the mice in the Ce6-APHPBs plus 660 nm group was 100% within 30 days, showing a good safety of Ce6-APHPBs in vivo (Figure 5D). In order to monitor the inhibitory effect of Ce6-APHPBs plus 660 nm on 4T1 tumors, we performed TUNEL staining of tumor sections at day 7 after treatment (Figure 5E). At day 14 post-treatment, H&E staining of tumor sections was conducted, which showed that the Ce6-APHPBs plus 660 nm group performed a significant killing effect on tumors (Figure 5F). To test whether these materials were toxic to normal tissues, we performed slices of heart, liver, spleen, lung and kidney from different groups of mice at day 14 after treatment and found that there was no significant structural damage (Figure 6A). Subsequent blood tests and blood biochemistry further demonstrated that Ce6-APHPBs were biologically safe (Figure 6B). Furthermore, there was no significant change in the body weight of the mice throughout the treatment (Figure S2). Because of the enzymatic catalytic activity of Ce6-APHPBs breaking down the hydrogen peroxide overexpressed in the tumor microenvironment into oxygen, the



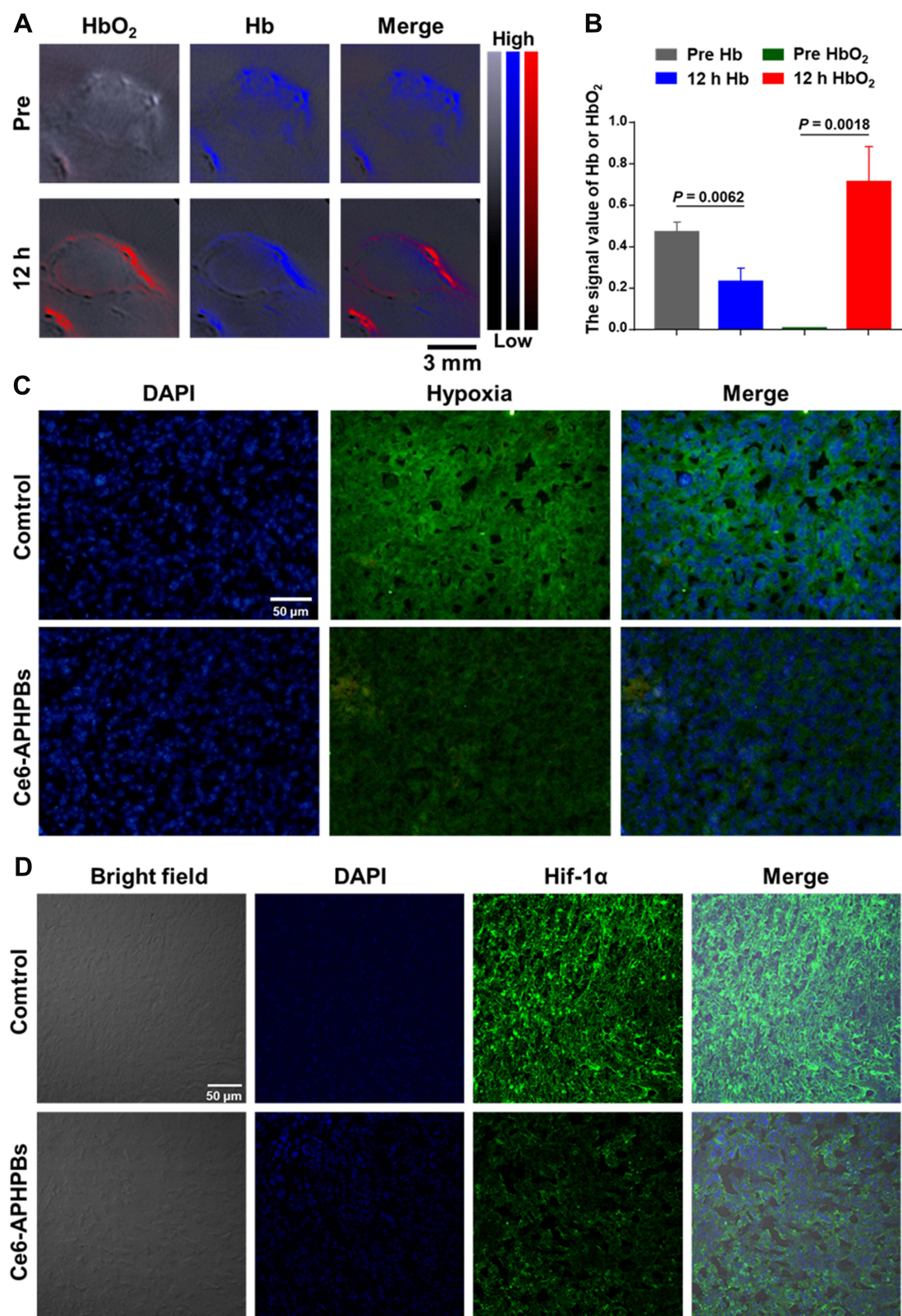


**Figure 4** (A) Photoacoustic imaging showing tumors deoxyhemoglobin (Hb) and oxyhemoglobin (HbO<sub>2</sub>) preinjection and i.v. injection of Ce6-APHPBs (2 mg/mL, 200 μL) at 12 h. (B) Statistical data of the signal value of Hb or HbO<sub>2</sub> at 12 h. Error bars represent the mean ± s.d. (n = 3). (C) Confocal hypoxia-fluorescence images of tumor slices collected from mice 12 h post-i.v. injection of PBS or Ce6-APHPBs (2 mg/mL, 200 μL). The cell nuclei and hypoxic areas were stained with DAPI (blue) and anti-pimonidazole antibody (FITC-green). (D) Immunofluorescence slices of HIF-1α expression in tumors (blue: nucleus, green: HIF-1α). Scale bar: 50 μm. P values in b were calculated by multiple t tests (\*\*P < 0.01).

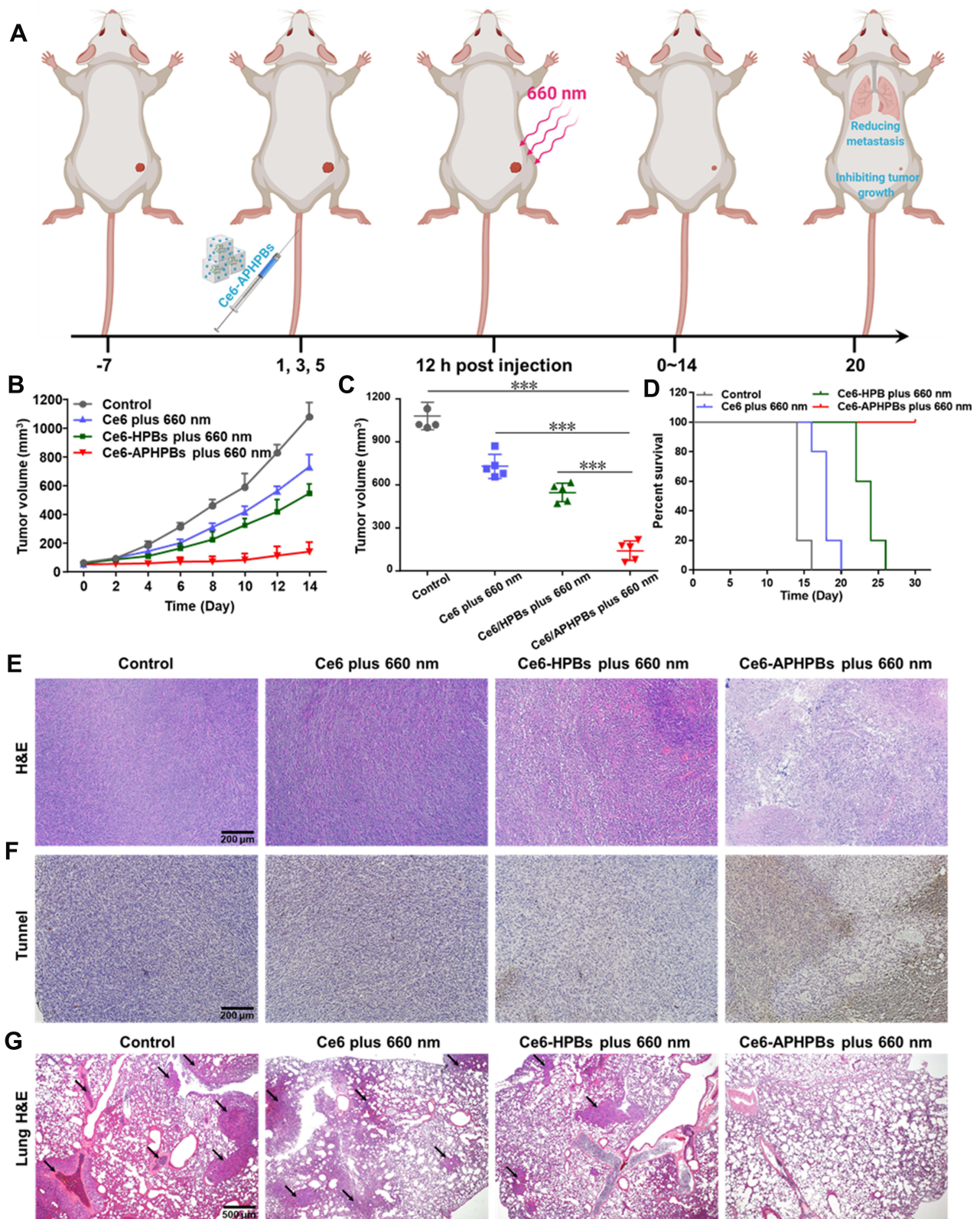


**Figure 5** (A) Schematic diagram of Ce6-APHPBs suppressing the growth of tumors and reducing metastasis to the lung. Created with BioRender.com. (B) Tumor growth curves measured for 14 days and (C) tumor volume at day 14 after different treatments. (D) Mouse survival curve in each group 30 days after treatments. Error bars represent mean ± s.d. (E) Hematoxylin and eosin (H&E)-stained tumor slices after intravenous injection in various groups at 7 days. (F) TUNEL-stained tumor slices of different groups at 7 days post-treatment. Scale bar: 200 μm. (G) H&E-stained lung slices of mice after various treatments at 20 days. Scale bar: 500 μm. P values in c were calculated by multiple t tests (\*\*\*) ( $P < 0.001$ ). (Ce6: 80 μg/mL, Ce6-HPBs: 2 mg/mL, Ce6-APHPBs: 2 mg/mL, 200 μL for each injection, irradiation time: 16 min at a time).



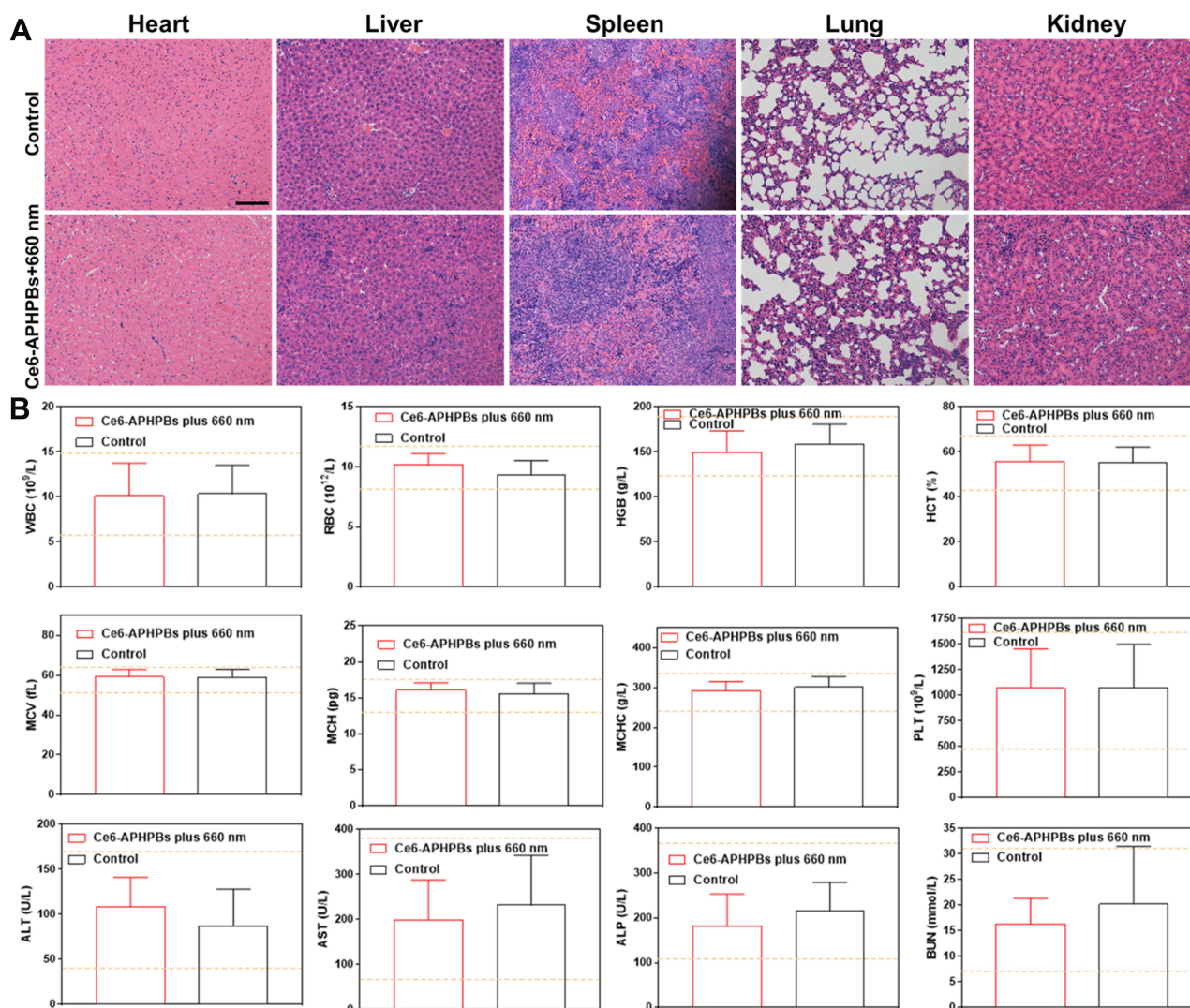


**Figure 6** In vivo biosafety analysis of enhanced PDT by Ce6-APHPBs. (A) Typical hematoxylin-eosin (H&E)-stained slice imaging of main organs, including the liver, spleen, kidney, lung and heart, gathered on day 10 after i.v. injection of Ce6-APHPBs+660 nm. (B) Blood biochemical and hematological data (including white blood cells (WBCs), red blood cells (RBCs), hemoglobin (HGB), hematocrit (HCT), mean cell volume (MCV), mean cell hemoglobin (MCH), and mean cell hemoglobin concentration (MCHC)). Blood urea nitrogen (BUN), alanine aminotransferase (ALT), alkaline phosphatase (ALP) and aspartate aminotransferase (AST) levels in BALB-c mice on day 10 after Ce6-APHPBs+660 nm injection (5 mice per group). Scale bar: 100  $\mu$ m.

PDT effect produced by the photosensitizer Ce6 was further enhanced. Lungs from different groups of mice were stained with H&E at day 20 post treatment. As shown in (Figure 5G), the Ce6-APHPB plus 660 nm group effectively reduced the metastasis to the lung.

## Conclusions

In our design, we constructed a photosensitizer loaded nano-zyme based on hollow Prussian blue (Ce6-APHPBs), which can not only effectively catalyze  $H_2O_2$  to produce  $O_2$  in TME, but also can further convert  $O_2$  into ROS to kill tumor cells under 660 nm laser irradiation. Especially in solid tumors, under the assistant of Ce6-APHPBs, the limitation of  $O_2$  dependence of PDT can be unfroze and the expression of HIF-1 $\alpha$  is reduced during the treatment at the same time, which further reduce the metastasis of tumor lesions. In a word, the novel Au-Pt nanozymes based hollow Prussian blue nanoparticles designed by us provide a new strategy and method for the PDT of clinical metastatic tumors. At the same time, the improvement of TME is crucial in tumor therapy, and our strategy also explores a new path for tumor therapy based on TME regulation.

## Acknowledgments

This work was supported by the Project of “Six Talent Peaks” in Jiangsu Province (NO. WSW-264), the “311 Project” of Taizhou City (NO. RCPY201813), Hospital Level Project of Taizhou People’s Hospital (NO. ZL202034, ZL202009) and Oncology Innovation Team Fund of Taizhou People’s Hospital.

## Disclosure

The authors declare no competing interests in this work.

## References

1. Kong XY, Cheng R, Wang J, Fang Y, Hwang KC. Nanomedicines inhibiting tumor metastasis and recurrence and their clinical applications. *Nano Today*. 2021;36:e23.
2. Park CG, Hartl CA, Schmid D, Carmona EM, Kim HJ, Goldberg MS. Extended release of perioperative immunotherapy prevents tumor recurrence and eliminates metastases. *Sci Transl Med*. 2018;10(433). doi:10.1126/scitranslmed.aar1916
3. Pei P, Shen WH, Zhou HL, et al. Radionuclide labeled gold nanoclusters boost effective anti-tumor immunity for augmented radio-immunotherapy of cancer. *Nano Today*. 2021;38:101144. doi:10.1016/j.nantod.2021.101144
4. Butturini E, Carcereri de Prati A, Boriero D, Mariotto S. Tumor dormancy and interplay with hypoxic tumor microenvironment. *Int J Mol Sci*. 2019;20(17):4305. doi:10.3390/ijms20174305
5. Emami Nejad A, Najafgholian S, Rostami A, et al. The role of hypoxia in the tumor microenvironment and development of cancer stem cell: a novel approach to developing treatment. *Cancer Cell Int*. 2021;21(1):62. doi:10.1186/s12935-020-01719-5
6. Fu R, Du W, Ding Z, et al. HIF-1 $\alpha$  promoted vasculogenic mimicry formation in lung adenocarcinoma through NRP1 upregulation in the hypoxic tumor microenvironment. *Cell Death Dis*. 2021;12(4):394. doi:10.1038/s41419-021-03682-z
7. Pei P, Shen W, Zhang Y, et al. Radioactive nano-oxygen generator enhance anti-tumor radio-immunotherapy by regulating tumor microenvironment and reducing proliferation. *Biomaterials*. 2022;280:121326. doi:10.1016/j.biomaterials.2021.121326
8. Tao J, Yang G, Zhou W, et al. Targeting hypoxic tumor microenvironment in pancreatic cancer. *J Hematol Oncol*. 2021;14(1):14.
9. Wang B, Zhao Q, Zhang Y, et al. Targeting hypoxia in the tumor microenvironment: a potential strategy to improve cancer immunotherapy. *J Exp Clin Cancer Res*. 2021;40(1):24. doi:10.1186/s13046-020-01820-7
10. Lu J. The Warburg metabolism fuels tumor metastasis. *Cancer Metastasis Rev*. 2019;38(1–2):157–164. doi:10.1007/s10555-019-09794-5
11. Song C, Phuengkham H, Kim YS, et al. Syringeable immunotherapeutic nanogel reshapes tumor microenvironment and prevents tumor metastasis and recurrence. *Nat Commun*. 2019;10(1):3745. doi:10.1038/s41467-019-11730-8
12. Yu Z, Zhou P, Pan W, Li N, Tang B. A biomimetic nanoreactor for synergistic chemiexcited photodynamic therapy and starvation therapy against tumor metastasis. *Nat Commun*. 2018;9(1):5044. doi:10.1038/s41467-018-07197-8
13. Li X, Zhou Z, Zhou R, et al. Stimuli-responsive nanoparticles combining photodynamic therapy and mitochondria disruption suppressed tumor metastasis. *Adv Mater Interfaces*. 2021;8(10):456.
14. Pei P, Sun C, Tao W, Li J, Yang X, Wang J. ROS-sensitive thioketal-linked polyphosphoester-doxorubicin conjugate for precise phototriggered locoregional chemotherapy. *Biomaterials*. 2019;188:74–82. doi:10.1016/j.biomaterials.2018.10.010
15. Yang J, Hou M, Sun W, et al. Sequential PDT and PTT using dual-modal single-walled carbon nanohorns synergistically promote systemic immune responses against tumor metastasis and relapse. *Adv Sci*. 2020;7(16):2001088. doi:10.1002/advs.202001088
16. Yue D, Cai X, Fan M, et al. An alternating irradiation strategy-driven combination therapy of PDT and RNAi for highly efficient inhibition of tumor growth and metastasis. *Adv Healthc Mater*. 2021;10(8):e2001850. doi:10.1002/adhm.202001850
17. Zeng JY, Zou MZ, Zhang MK, et al. pi-Extended benzoporphyrin-based metal-organic framework for inhibition of tumor metastasis. *Acs Nano*. 2018;12(5):4630–4640. doi:10.1021/acsnano.8b01186
18. Ma Y, Ma Y, Gao M, et al. Platelet-mimicking therapeutic system for noninvasive mitigation of the progression of atherosclerotic plaques. *Adv Sci*. 2021;8(8):2004128. doi:10.1002/advs.202004128
19. Sobhani N, Samadani AA. Implications of photodynamic cancer therapy: an overview of PDT mechanisms basically and practically. *J Egypt Natl Canc Inst*. 2021;33(1):34. doi:10.1186/s43046-021-00093-1
20. Wen L, Zhang Y, Zhang L, et al. Application of different noninvasive diagnostic techniques used in HMME-PDT in the treatment of port wine stains. *Photodiagnosis Photodyn Ther*. 2019;25:369–375. doi:10.1016/j.pdpdt.2019.01.008
21. Wu W, Shi L, Duan Y, et al. Nanobody modified high-performance AIE photosensitizer nanoparticles for precise photodynamic oral cancer therapy of patient-derived tumor xenograft. *Biomaterials*. 2021;274:120870. doi:10.1016/j.biomaterials.2021.120870
22. Fan GL, Deng FA, Zhou X, et al. Plasma membrane targeted photodynamic O<sub>2</sub> economizer for hypoxic tumor therapy. *Biomaterials*. 2021;273:120854. doi:10.1016/j.biomaterials.2021.120854
23. Liu Z, Xie Z, Li W, et al. Photodynamic immunotherapy of cancers based on nanotechnology: recent advances and future challenges. *J Nanobiotechnology*. 2021;19(1):160. doi:10.1186/s12951-021-00903-7
24. Sun Y, Zhao D, Wang G, et al. Recent progress of hypoxia-modulated multifunctional nanomedicines to enhance photodynamic therapy: opportunities, challenges, and future development. *Acta Pharm Sin B*. 2020;10(8):1382–1396. doi:10.1016/j.apsb.2020.01.004
25. Yang Z, Wang J, Ai S, Sun J, Mai X, Guan W. Self-generating oxygen enhanced mitochondrion-targeted photodynamic therapy for tumor treatment with hypoxia scavenging. *Theranostics*. 2019;9(23):6809–6823. doi:10.7150/thno.36988
26. Li Y, Wu CJ, Zhai YW, et al. Palliating the escalated post-PDT tumor hypoxia with a dual cascade oxygenation nanocomplex. *Appl Mater Today*. 2022;26. doi:10.1016/j.apmt.2021.101337
27. Shi L, Hu F, Duan Y, et al. Hybrid nanospheres to overcome hypoxia and intrinsic oxidative resistance for enhanced photodynamic therapy. *Acs Nano*. 2020;14(2):2183–2190. doi:10.1021/acsnano.9b09032
28. Gulzar A, Xu JT, Wang C, et al. Tumour microenvironment responsive nanoconstructs for cancer theranostic. *Nano Today*. 2019;26:16–56.

29. Tang W, Yang Z, He L, et al. A hybrid semiconducting organosilica-based O<sub>2</sub> nanoeconomizer for on-demand synergistic photothermally boosted radiotherapy. *Nat Commun.* 2021;12(1):523. doi:10.1038/s41467-020-20860-3
30. Yang N, Xiao W, Song X, Wang W, Dong X. Recent advances in tumor microenvironment hydrogen peroxide-responsive materials for cancer photodynamic therapy. *Nanomicro Lett.* 2020;12(1):15. doi:10.3847/1538-4357/ab5f08
31. Zhu P, Chen Y, Shi J. Nanoenzyme-augmented cancer sonodynamic therapy by catalytic tumor oxygenation. *Acs Nano.* 2018;12(4):3780–3795. doi:10.1021/acsnano.8b00999
32. Zeng Z, Zhang C, Li J, Cui D, Jiang Y, Pu K. Activatable polymer nanoenzymes for photodynamic immunometabolic cancer therapy. *Adv Mater.* 2021;33(4):e2007247.
33. Dacarro G, Taglietti A, Pallavicini P. Prussian blue nanoparticles as a versatile photothermal tool. *Molecules.* 2018;23(6):1414. doi:10.3390/molecules23061414
34. Zhang W, Hu S, Yin JJ, et al. Prussian blue nanoparticles as multienzyme mimetics and reactive oxygen species scavengers. *J Am Chem Soc.* 2016;138(18):5860–5865. doi:10.1021/jacs.5b12070
35. Hang L, Li H, Zhang T, et al. Au@Prussian blue hybrid nanomaterial synergy with a chemotherapeutic drug for tumor diagnosis and chemodynamic therapy. *ACS Appl Mater Interfaces.* 2019;11(43):39493–39502. doi:10.1021/acscami.9b13470
36. Yang ZL, Tian W, Wang Q, et al. Oxygen-evolving mesoporous organosilica coated prussian blue nanoplatfor for highly efficient photodynamic therapy of tumors. *Adv Sci.* 2018;5(5):1700847. doi:10.1002/advs.201700847
37. Lu L, Zhang C, Zou B, Wang Y. Hollow prussian blue nanospheres for photothermal/chemo-synergistic therapy. *Int J Nanomedicine.* 2020;15:5165–5177. doi:10.2147/IJN.S252505
38. Qin Z, Li Y, Gu N. Progress in applications of prussian blue nanoparticles in biomedicine. *Adv Healthc Mater.* 2018;7(20):e1800347. doi:10.1002/adhm.201800347
39. Ren C, Cheng Y, Li W, et al. Ultra-small Bi<sub>2</sub>S<sub>3</sub> nanodot-doped reversible Fe(ii/iii)-based hollow mesoporous Prussian blue nanocubes for amplified tumor oxidative stress-augmented photo-/radiotherapy. *Biomater Sci.* 2020;8(7):1981–1995. doi:10.1039/C9BM02014D
40. Shou P, Yu Z, Wu Y, et al. Zn(2+) doped ultrasmall prussian blue nanotheranostic agent for breast cancer photothermal therapy under MR imaging guidance. *Adv Healthc Mater.* 2020;9(1):e1900948. doi:10.1002/adhm.201900948
41. Wang X, Li H, Li F, Han X, Chen G. Prussian blue-coated lanthanide-doped core/shell/shell nanocrystals for NIR-II image-guided photothermal therapy. *Nanoscale.* 2019;11(45):22079–22088. doi:10.1039/C9NR07973D
42. Zhang K, Tu M, Gao W, et al. Hollow prussian blue nanozymes drive neuroprotection against ischemic stroke via attenuating oxidative stress, counteracting inflammation, and suppressing cell apoptosis. *Nano Lett.* 2019;19(5):2812–2823. doi:10.1021/acs.nanolett.8b04729
43. Gao X, Wang Q, Cheng C, et al. The application of prussian blue nanoparticles in tumor diagnosis and treatment. *Sensors.* 2020;20(23):6905. doi:10.3390/s20236905
44. Wang S, Yan H, Wang Y, Wang N, Lin Y, Li M. Hollow Prussian Blue nanocubes as peroxidase mimetic and enzyme carriers for colorimetric determination of ethanol. *Mikrochim Acta.* 2019;186(11):738. doi:10.1007/s00604-019-3826-6

International Journal of Nanomedicine

Dovepress

## Publish your work in this journal

The International Journal of Nanomedicine is an international, peer-reviewed journal focusing on the application of nanotechnology in diagnostics, therapeutics, and drug delivery systems throughout the biomedical field. This journal is indexed on PubMed Central, MedLine, CAS, SciSearch®, Current Contents®/Clinical Medicine, Journal Citation Reports/Science Edition, EMBase, Scopus and the Elsevier Bibliographic databases. The manuscript management system is completely online and includes a very quick and fair peer-review system, which is all easy to use. Visit <http://www.dovepress.com/testimonials.php> to read real quotes from published authors.

Submit your manuscript here: <https://www.dovepress.com/international-journal-of-nanomedicine-journal>